tract-treated embryos had 3571 ± 456 (n = 5); controls had 2567 ± 380 (n = 6) ($P < 0.01$, t test).
15. I. Chu-Wang and R. W. Oppenheim, *J. Comp. Neurol.* **177**, 33 (1978).
16. E8 embryos treated with partially purified hindlimb extract (25 to 75% $AmSO_4$ fraction) beginning on E5 had 7.2 ± 1.3 (n = 5) pyknotic motoneuron profiles per 1000 healthy neurons in the eight lumbar segments; controls had 18.0 ± 2.3 (n = 5) ($P < 0.001$, t test). Pyknotic motoneurons were identified by established criteria (*15*). Care was used to exclude degenerating glia and mitotic figures.
17. Embryos were treated daily beginning on E6 with partially purified hindlimb extract (25 to 75% $AmSO_4$ fraction, 3 mg of protein per milliliter) prepared from either E9 or E16 embryos. Motoneuron counts (mean ± SEM) on E10 were 12,256 ± 231 (n = 10) for controls and 15,303 ± 256 (n = 10) for E9 extract-treated, and 10,500 ± 187 (n = 6) for E16 extract-treated embryos. The E16 group was significantly different from both control ($P < 0.05$, t test) and E9 extract-treated ($P < 0.01$) groups. Control and E9 extract-treated groups were also significantly different ($P < 0.01$). Embryos treated with E9 extract had significantly fewer pyknotic motoneurons per 1000 healthy motoneurons on E10 than either the embryos treated with E16 extract or control embryos. Means ± SEM were 1.3 ± 0.5 for E9 extract, 3.3 ± 1.1 for E16 extract, and 3.5 ± 0.9 for controls ($P < 0.01$, t test).
18. R. W. Oppenheim, I. Chu-Wang, J. L. Maderdrut, *J. Comp. Neurol.* **177**, 87 (1978).
19. M. E. Lanser, J. L. Carrington, J. F. Fallon, *J. Neurosci.* **6**, 2551 (1986); M. E. Lanser and J. F. Fallon, *J. Comp. Neurol.* **261**, 423 (1987).
20. M. E. Gurney *et al.*, *Science* **234**, 566 (1986).
21. M. A. Hill and M. R. Bennett, *Neurosci. Lett.* **35**, 31 (1983); *Dev. Brain Res.* **24**, 305 (1986).
22. V. Hamburger and H. Hamilton, *J. Morphol.* **88**, 49 (1951).
23. B. K. Smith *et al.*, *Anal. Biochem.* **150**, 76 (1985).
24. S. Udenfriend *et al.*, *Science* **178**, 871 (1972).
25. R. W. Oppenheim, J. Maderdrut, D. Wells, *J. Comp. Neurol.* **210**, 174 (1982).
26. We thank S. McKay for technical assistance. Supported by NIH grants NS 20402 (R.W.O.), NS 23058 (J.L.M.), the Muscular Dystrophy Association, and California Biotechnology, Inc.

10 November 1987; accepted 22 March 1988

Theoretical Studies of DNA During Gel Electrophoresis

J. M. DEUTSCH

A numerical study of the motion of a long-chain macromolecule in a gel has shown unexpected features. The application of a field appears to induce the chain to contract on itself. This is followed by its "unwinding" into an extended configuration. For long chains, the mobility tends toward a constant, in accord with experiments. For the parameter range used, the observed molecular motion differs strongly from assumptions made in the present theory of electrophoresis.

GEL ELECTROPHORESIS IS A WIDELY used technique for separating macromolecules according to size. There have been many substantive improvements in this technique recently (*1–3*) that allow the separation of much larger DNA molecules than was previously possible. Still, the basic underlying motion of the molecules has remained somewhat of a mystery.

The most successful theory of electrophoresis has made use of the concept of a "tube" (*4*) through which the chain passes. The resultant idealized motion, called "reptation," has been successfully applied to situations involving diffusion where no external electric field is present. Several groups (*5*) have extended this theory to the case where a uniform external field is applied. The extension is not entirely straightforward, and certain statistics for the tube must be postulated (*5*). It is further assumed that the overall tube length fluctuates little.

Experimental data for the constant field case (*6*) supports tube theories. On the other hand, a more recent technique of electrophoretic separation that periodically inverts the direction of the electric field (*2*) leads to very different mobilities than for the constant field case. This is not predicted by tube models, which give the same dependence of mobility versus chain length as in the constant field case.

There are qualitative differences between the predictions of the tube models and the results described here, which were obtained by direct numerical solution of equations describing the motion of the chain. These equations (defined below) contain far fewer assumptions than present tube theories, although various simplifications have still been made. Namely, intrachain repulsion and effects of gel heterogeneity have not been included. A uniform distribution of charge along the chain has also been assumed. To critically compare tube theories with the numerical results, it is only practical to start with a more basic but still rather idealized model.

Consider Fig. 1A. Here one sees a chain made up of N beads on freely hinged links moving in a two-dimensional lattice of obstacles that represents the gel. There is a short-range repulsive force $\mathbf{F}_i$, between each obstacle and all beads on the chain. This force completely prohibits the chain crossing an obstacle. The effects of temperature are represented by a Gaussian random force that acts on each bead independently. More precisely, the following Langevin equation was solved numerically (*7*):

$$\nu \frac{\partial \mathbf{r}_i}{\partial_t} = \mathbf{T}_{i,i+1} - \mathbf{T}_{i,i-1} + q\mathbf{E} + \mathbf{F}_i + \mathbf{f}_i$$

Here ν is the friction coefficient between the ith bead and the solvent, $\mathbf{r}_i$ is the vector coordinate, t is time, $\mathbf{T}_{i,j}$ is the tension between adjacent beads i and j, q is the charge on a bead, $\mathbf{E}$ is the electric field, and $\mathbf{f}_i$ is the random force acting on bead i. The tensions are determined by the requirement that the distance between two adjacent beads remain constant and equal to l, that is, $(\mathbf{r}_{i+1} - \mathbf{r}_i)^2 = l^2$.

The case of experimental interest is where the pore size (that is, the lattice spacing) is

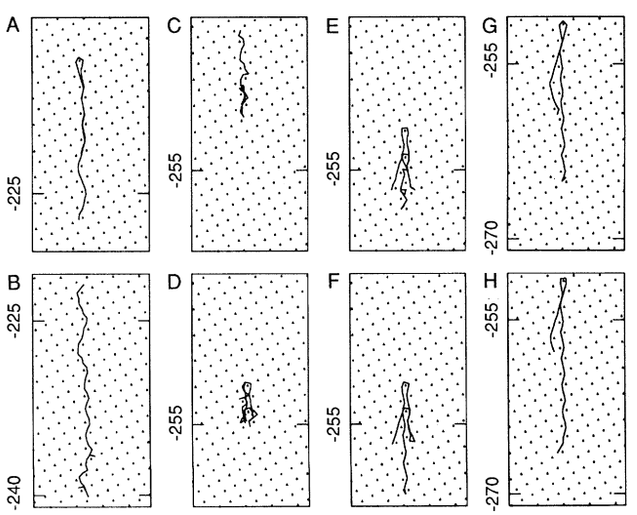

Fig. 1. The evolution of a DNA molecule in a gel. This sequence shows the different stages described in the text. The parameters in this run were qEl/k_BT = 42.67. The relative times for each frame are (**A**) 100, (**B**) 105, (**C**) 110, (**D**) 112, (**E**) 114, (**F**) 116, (**G**) 118, and (**H**) 119. The direction of the electric field is vertically downward.

Department of Physics, University of California, Santa Cruz, CA 95064.

near the persistence length (l). Hence the simulations described below are in this category (lattice spacing = 2.128 × l). For nonzero but low temperature or high electric field, that is, $qEl/k_BT > 5$, where k_B is Boltzmann's constant, the main features of the motion can be characterized by the following stages:

1) Starting from Fig. 1A, a chain moves downwards in the direction of the electric field. It is hooked around an obstacle and appears almost fully extended.

2) The chain slides off the obstacle and begins to contract. Note that the front of the chain is more coiled than the back (Fig. 1B).

3) The front of the chain curls up into a rather dense ball, with a lower mobility than the trailing portions of the chain (Fig. 1C).

4) Eventually the entire chain is compressed into the ball at the front, and the chain becomes jammed in between obstacles (Fig. 1D).

5) The chain begins unwinding around the obstacles. The chain may be hooked in several places around different obstacles (Fig. 1, E and F).

At this point (Fig. 1, G and H), the chain is back at stage 1 (Fig. 1A) and the whole process repeats (*8*). Note that tube models assume that typical configurations look like Fig. 1B and that all of the other configurations in Fig. 1 are assumed to occur extremely infrequently. The main features of motion can be understood qualitatively starting with stage 1. Here the chain is hooked around some obstacles and is slipping off in the direction of the longer side. One can easily calculate the tension in different portions of the chain. For most experimental situations (as in this simulation), $N^2qEl/k_BT > 1$, in which case the tension suppresses thermal fluctuations so that the chain remains almost completely taut for all but the last few segments of chain. This explains why the chain becomes so extended by the obstacles and begins to contract only when it has almost completely disengaged from the obstacle.

Stages 2, 3, and 4 clearly represent an instability, the cause of which is apparent by detailed inspection of the motion. The leading edge of the chain is moving slower than the rest of the chain because there is an additional friction due to the chain colliding with obstacles. The more the front of the chain becomes coiled up, the thicker the tube becomes in the direction perpendicular to the field. The standard reptation model (*4*) can be modified to incorporate this effect by introducing a friction coefficient that depends on the local chain conformation. Numerical solution of this model indeed shows the same instability (*9*).

The unwinding motion of stage 5 is similar to a model devised by the author in the context of orthogonal pulsed field electrophoresis (*10*). In most cases, the chain will unwind around the obstacle to a configuration such as stage 1 in a time that scales as $Nlv/(qE)$. In rare instances, one finds "chain pinning" when the two sides of the chain are almost equal in length. In this case the chain remains trapped around the obstacles for a very long time that scales as $\exp(qEl/k_BT)$ (*10*). Chain pinning on a somewhat shorter time scale occurs naturally within the framework of the reptation model as well (*11*).

When E is further reduced such that $qEl/k_BT < 5$, the behavior becomes more complex (Fig. 2), the motion still being qualitatively different from tube models. Instead of the coiling process occurring at the leading end, as usually happens for the parameter range discussed above, coiling often appears in the middle of the chain, frequently leading to an instability in which the upper half of the chain reorients to give rise to an inverted u shape.

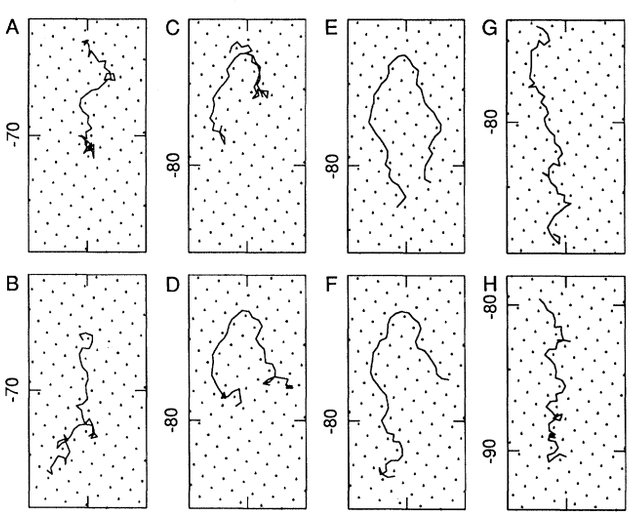

Fig. 2. For much lower fields ($qEl/k_BT < 5$), the motion takes a different form illustrated here ($qEl/k_BT = 0.604$). The relative times for each frame shown are (**A**) 260, (**B**) 270, (**C**) 280, (**D**) 290, (**E**) 330, (**F**) 340, (**G**) 350, and (**H**) 360. The electric field is vertically downward.

Now I address the relation between this simulation and experiment. Figure 3 shows the mobility versus chain length for simulations at three different electric fields. The mobility of an unimpeded chain, that is, a chain where all of the obstacles have been removed, is 100 on the vertical scale. It is clear that the mobility has the same general features as found experimentally. Most notably, the mobility plateaus to a constant for long chains. The reason for this is straightforward and follows from simple scaling. The detailed assumptions of the reptation model do not appear necessary to obtain this result. In addition, the mobility in the simulations saturates at high fields, in accord with experiments.

Experimental data on the birefringence of DNA under the sudden application of an electric field shows an overshoot and then an undershoot before it reaches steady state (*12*). These features are interpretable as oscillations between stretched and collapsed chains, in accordance with the above results. Numerical data on field inversion gel electrophoresis shows a minimum in the mobility as a function of inversion frequency (*9*), also in accord with experiment (*2*). If the chain starts in a configuration similar to Fig. 2C, the motion downward is slower than if the field is suddenly reversed because of the high tension the chain is under when it moves downward. Although the DNA spends only a third of the time moving upward, its center of mass moves upward at roughly twice the speed as for moving downward. Therefore the DNA remains hooked around the obstacles for a long period of time.

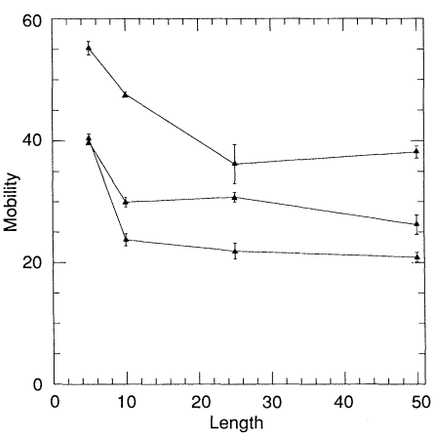

Fig. 3. The mobility versus chain length at three different field strengths (mobility = 100 for an unimpeded chain). For the bottom curve, $qEl/k_BT = 0.604$, for the middle curve $qEl/k_BT = 1.208$, and for the top curve, $qEl/k_BT = 42.67$. (Note that the top curve was run at one-eighth the temperature of the bottom two curves.) The error bars show a 95% confidence interval. The distance moved at the end of one run was always greater than four chain lengths.

There are two constructive outcomes of the above findings. First, for the parameter range used, chain motion can be characterized by several stages, all of which appear amenable to theoretical treatment (*9, 10*). Second, unlike tube models, the case of reverse field electrophoresis is not expected to give the same dependence of mobility versus chain length as the constant field case.

REFERENCES AND NOTES

1. D. C. Schwartz and C. R. Cantor, *Cell* **37**, 67 (1984).
2. G. F. Carle, M. Frank, M. V. Olson, *Science* **232**, 65 (1986).
3. G. Chu, D. Vollrath, R. W. Davis, *ibid.* **234**, 1582 (1986).
4. P. G. de Gennes, *J. Chem. Phys.* **55**, 572 (1971).
5. L. S. Lerman and H. L. Frisch, *Biopolymers* **21**, 995 (1982); O. J. Lumpkin and B. H. Zimm, *ibid.*, p. 2315; C. P. Bean and H. Hervet, *Biophys. J.* **41**, A289 (1983); O. J. Lumpkin, P. Dejardin, B. H. Zimm, *Biopolymers* **24**, 1575 (1985); G. W. Slater and J. Noolandi, *ibid.*, p. 2181.
6. H. Hervet and C. P. Bean, *Biopolymers* **26**, 727 (1987).
7. Monte Carlo techniques, which have been used successfully in many polymer systems, do not work here; see M. Olvera de la Cruz, J. M. Deutsch, S. F. Edwards, *Phys. Rev. A* **33**, 2047 (1986). The Langevin equation used has a more fundamental status than Monte Carlo simulations.
8. It is important to note that stage 1 is not an initial condition. The above cycle represents the steady-state behavior of the chain and is independent of the details of the initial condition.
9. J. M. Deutsch and T. L. Madden, unpublished results.
10. J. M. Deutsch, *Phys. Rev. Lett.* **59**, 1255 (1987).
11. J. Noolandi, J. Rousseau, G. W. Slater, C. Turmal, M. Lalande, *ibid.* **58**, 2428 (1987).
12. G. Holzwarth, C. B. McKee, S. Steiger, G. Crater, *Nucleic Acids Res.* **15**, 10031 (1987).

13. The author thanks T. L. Madden for useful discussions. Supported by NSF grant DMR 84-19536.

21 December 1987; accepted 28 March 1988

Iron-Responsive Elements: Regulatory RNA Sequences That Control mRNA Levels and Translation

JOHN L. CASEY, MATTHIAS W. HENTZE, DAVID M. KOELLER, S. WRIGHT CAUGHMAN, TRACEY A. ROUAULT, RICHARD D. KLAUSNER, JOE B. HARFORD

The biosynthetic rates for both the transferrin receptor (TfR) and ferritin are regulated by iron. An iron-responsive element (IRE) in the 5′ untranslated portion of the ferritin messenger RNA (mRNA) mediates iron-dependent control of its translation. In this report the 3′ untranslated region of the mRNA for the human TfR was shown to be necessary and sufficient for iron-dependent control of mRNA levels. Deletion studies identified a 678-nucleotide fragment of the TfR complementary DNA that is critical for this iron regulation. Five potential stem-loops that resemble the ferritin IRE are contained within the region critical for TfR regulation. Each of two of the five TfR elements was independently inserted into the 5′ untranslated region of an indicator gene transcript. In this location they conferred iron regulation of translation. Thus, an mRNA element has been implicated in the mediation of distinct regulatory phenomena dependent on the context of the element within the transcript.

IN PROLIFERATING CELLS, THE AVAILability of iron modulates the biosynthetic rates for at least two proteins critical to cellular iron metabolism. The transferrin receptor (TfR) serves as the chief means of iron uptake, and its biosynthesis is decreased when iron is abundant and increased when it is scarce (*1*). Conversely, ferritin, which sequesters iron in the cytoplasm, is synthesized at a higher rate when iron is abundant than when it is scarce (*2*). The mechanisms involved in the control of the biosynthetic rates for these two proteins are distinct. For the TfR the regulation of biosynthetic rates can be accounted for by changes in mRNA levels (*3*). In contrast, ferritin biosynthesis is altered without a corresponding change in the level of total ferritin mRNA (*4*) by redistribution of mRNA between polysome and nonpolysome pools (*5*).

The iron-dependent modulation of the level of TfR mRNA is mediated by two regions of the gene. Together these two regions can produce >20-fold differences in transcript levels between cells treated with an iron chelator and those treated with an iron source. The transcription rate directed by 5′ flanking sequences of the TfR gene is two- to threefold higher in cells treated with the iron chelator desferrioxamine than in cells treated with hemin, an iron source (*6*). However, deletion of sequences corresponding to the 3′ untranslated region (3′UTR) of the TfR mRNA eliminates most of the iron regulation of transcript levels regardless of whether the TfR promoter region is present (*6, 7*).

The 5′ untranslated region (5′UTR) of human ferritin H chain mRNA is both necessary and sufficient to mediate iron-responsive translational regulation of ferritin biosynthesis (*8*). Moreover, the specific sequence within the ferritin 5′UTR responsible for the modulation of ferritin translation has been identified (*9, 10*). This RNA sequence, which we have termed an iron-responsive element (IRE), has the potential to form a characteristic stem-loop structure. The 5′UTR of each ferritin gene for which complete mRNA sequence data are available [human (*11*), rat (*12*), chicken (*13*), and frog (*14*)] contains a sequence capable of forming a similar stem-loop. Here we present a deletion analysis of the TfR 3′UTR that implicates strikingly similar elements in the iron-responsive regulation of TfR mRNA levels. We further show that synthetic oligonucleotides corresponding to elements of the TfR 3′UTR confer ferritin-like translational regulation when inserted in the 5′UTR of an indicator gene transcript.

We (*6*) and others (*7*) have shown that the sequences corresponding to the 3′UTR of the TfR mRNA are necessary for the full degree of iron regulation of the level of this transcript. To demonstrate the sufficiency of this region to confer TfR-like iron regulation on another gene, we have inserted a fragment containing most (2.2 kb of 2.5 kb) of the TfR 3′UTR into the 3′UTR of the structural gene for human growth hormone (hGH) and have transformed murine cells with this construct (pSVGH-TR). The hybrid construct gave rise to three major hGH/

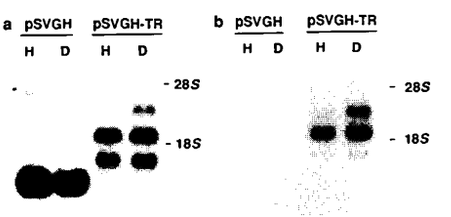

Fig. 1. The 3′UTR of the human transferrin receptor is sufficient to confer iron regulation on the accumulation of a chimeric transcript. Pools of stable transformants were prepared as described (*6*) after transfection with pSVGH or pSVGH-TR as indicated (*17*). Cells were treated for 16 hours with 6 m*M* sodium butyrate plus either 100 μ*M* hemin (H) or 100 μ*M* desferrioxamine (D) prior to isolation of cytoplasmic RNA (*6*). RNA was separated by electrophoresis in a 1% agarose-formaldehyde gel and analyzed by blot hybridization with an hGH probe consisting of the 650-bp Sty I fragment of the hGH gene (**a**) or the full-length human TfR cDNA (*18*) (**b**). The relative positions of the 28*S* and 18*S* ribosomal RNAs are indicated.

Cell Biology and Metabolism Branch, National Institute of Child Health and Human Development, National Institutes of Health, Bethesda, MD 20892.